

# Targeted Delivery of Auristatin-Modified Toxins to Pancreatic Cancer Using Aptamers

Christina Kratschmer<sup>1</sup> and Matthew Levy<sup>1,2</sup>

<sup>1</sup>Department of Biochemistry, Albert Einstein College of Medicine, Bronx, NY, USA

**Pancreatic cancer is one of the most lethal malignancies. Treatment with the first-line agent, gemcitabine, is often unsuccessful because it, like other traditional chemotherapeutic agents, is non-specific, resulting in off-target effects that necessitate administration of subcurative doses. Alternatively, monomethyl auristatin E (MMAE) and monomethyl auristatin F (MMAF) are highly toxic small molecules that require ligand-targeted delivery. MMAE has already received FDA approval as a component of an anti-CD30 antibody-drug conjugate, brentuximab vedotin. However, in contrast to antibodies, aptamers have distinct advantages. They are chemicals, which allows them to be produced synthetically and facilitates the rapid development of diagnostics and therapeutics with clinical applicability. In addition, their small size allows for enhanced tissue distribution and rapid systemic clearance. Here, we assayed the toxicity of MMAE and MMAF conjugated to an anti-transferrin receptor aptamer, Waz, and an anti-epidermal growth factor receptor aptamer, E07, on the pancreatic cancer cell lines Panc-1, MIA PaCa-2, and BxPC3. *In vitro*, our results indicate that these aptamers are a viable option for the targeted delivery of toxic payloads to pancreatic cancer cells.**

## INTRODUCTION

Pancreatic cancer is the 4<sup>th</sup> leading cause of cancer death.<sup>1</sup> Pancreatic ductal adenocarcinoma (PDAC) is by far the most common subtype of pancreatic cancer, representing 90% of cases. A minority of patients (10%–15%) present with disease that is amenable to surgery, the only treatment that offers any hope of cure. However, even with adjuvant therapy (i.e., chemotherapy), 80% of these patients experience a relapse within 2 years of surgery.<sup>2</sup>

Most patients present with either locoregional disease that precludes surgery because of vascular invasion or advanced-stage disease with distant metastases. For patients with advanced disease, current therapy relies on gemcitabine as the first-line treatment, yet the benefit is modest.<sup>3</sup> Overall, this treatment regimen results in a 5 year survival rate of only 8%.<sup>1</sup> Numerous studies using novel cytotoxic agents and novel combinations of existing chemotherapies have failed to improve survival.<sup>4</sup> Disappointingly, PDAC is one of the few cancers with recent increases in incidence or mortality.<sup>1</sup> Because of the extremely aggressive nature of PDAC, in particular its propensity for distant metastasis and broad chemoresistance, there is an obvious need for the development of new therapies.

Advances in the field of antibody-drug conjugates (ADCs) have demonstrated the power of targeting potent cytotoxic drugs directly to cell surface receptors. The targeted delivery of small molecule cytotoxics, such as calicheamicin, has been replaced with newer classes of drugs, the maytansine and auristatin derivatives, both of which work by inhibiting microtubule assembly.<sup>5–7</sup> Due to the extreme potency of ADCs, achieving a therapeutic effect requires less than 1% of an injected dose to localize to tumors.<sup>8</sup> The development of emtansine, a maytansine derivative, led to U.S. Food and Drug Administration (FDA) approval of ado-trastuzumab emtansine (Kadcyla), an anti-HER2 ADC for the treatment of metastatic breast cancer.<sup>9</sup> In addition, in July 2011, brentuximab vedotin (Adcentris), an anti-CD30 monomethyl auristatin E (MMAE) ADC, was approved by the FDA for the treatment of Hodgkin's lymphoma and systemic anaplastic large-cell lymphoma.<sup>10</sup> In the case of PDAC, MMAE has also shown promise when conjugated to an anti-tissue factor antibody<sup>11</sup> and an anti-mesothelin antibody.<sup>12</sup> It has also shown efficacy as a sensitizer for ionizing radiation therapy.<sup>13</sup>

Targeting PDAC requires knowledge of cell-specific surface receptors, and although no magic bullets are known to hone exclusively to PDAC, the epidermal growth factor receptor (EGFR) and the transferrin receptor (TfR, CD71) have demonstrated high levels of expression on PDAC.<sup>14,15</sup> In addition, EGFR overexpression is associated with poor prognosis and disease progression,<sup>16</sup> while TfR overexpression supports malignant growth by modulating mitochondrial respiration and reactive oxygen species production.<sup>15,17</sup> Both receptors are internalized by clathrin-mediated endocytosis, suggesting a potential mechanism for delivery of toxins.

Work in the field of targeted delivery has focused largely on the use of antibodies; however, challenges in the field remain (reviewed in Donaghy<sup>8</sup>). Aptamers are single-stranded oligonucleotides selected to bind a target with high affinity and specificity. Their ability to be chemically synthesized facilitates toxin conjugation, and their small size may be optimal for tumor penetration. An anti-TfR aptamer, Waz, and an anti-EGFR aptamer, E07, have already been selected

Received 1 June 2017; accepted 26 November 2017;  
<https://doi.org/10.1016/j.omtn.2017.11.013>.

<sup>2</sup>Present address: Vitrisa Therapeutics, Durham, NC 27701, USA

**Correspondence:** Matthew Levy, Vitrisa Therapeutics, Durham, NC 27701, USA.  
**E-mail:** [mlevy@vitrisatherapeutics.com](mailto:mlevy@vitrisatherapeutics.com)



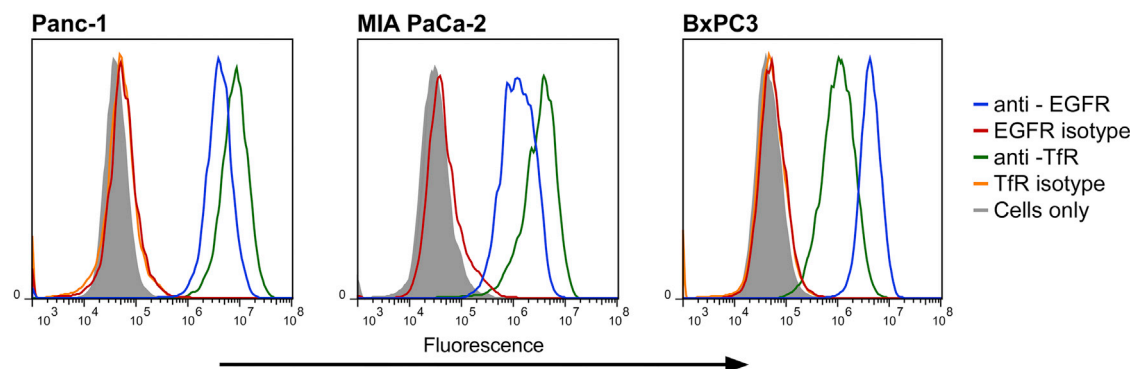


**Figure 1. Antibody Binding Characteristics of PDAC Cells**

Panc-1, MIA PaCa-2, and BxPC3 cells were stained with an anti-EGFR antibody (blue), an anti-TfR antibody (green), and appropriate isotype controls (red and orange, respectively).

and validated.<sup>18,19</sup> Furthermore, E07 has been used to deliver gemcitabine to the EGFR-expressing PDAC cell line MIA PaCa-2 to induce cell death.<sup>20</sup>

Previously, our lab demonstrated the ability to generate aptamer-toxin conjugates using a recombinant variant of the ribosomal toxin gelonin and the minimized anti-prostate-specific membrane antigen (PSMA) aptamer, A9.min.<sup>21</sup> Here, we assessed the ability to generate small molecule aptamer-toxin conjugates. Using thiol-reactive variants of the auristatin toxins MMAE and monomethyl auristatin F (MMAF), we generated aptamer-toxin conjugates using both the anti-EGFR aptamer, E07, and the anti-TfR aptamer, Waz, and tested their cytotoxicity on three distinct PDAC cell lines: Panc-1, MIA PaCa-2, and BxPC3. Our analysis takes advantage of the varying levels of expression of EGFR and TfR on these cells lines, as well as fundamental differences in the behavior of MMAE and MMAF.

## RESULTS

### Validation of Target Expression and Aptamer Binding on PDAC Cell Lines

The PDAC cell lines Panc-1, MIA PaCa-2, and BxPC3 are all reported to express TfR and EGFR.<sup>15,22,23</sup> To confirm this, we screened these cell lines for target receptor expression by flow cytometry using commercially available antibodies. Cells were incubated with phycoerythrin (PE)-labeled TfR and EGFR antibodies. After incubation, cells were washed and read by flow cytometry. As seen in Figure 1, all three PDAC cell lines express both TfR and EGFR, with Panc-1 and MIA PaCa-2 cells demonstrating higher expression levels of TfR and BxPC3 cells demonstrating higher levels of EGFR.

Having established target expression and the relative expression levels of these surface receptors, we assessed the ability to target and label these same cells using fluorescently labeled aptamers reported to target the same receptors. We chemically synthesized the anti-TfR aptamer, Waz; the anti-EGFR aptamer, E07; and a nontargeting control, C36, using standard solid-phase synthesis. Aptamers were synthesized

bearing a 3' inverted thymidine (dT) for increased stability and a 5' thiol for conjugation to the fluorescent molecule DyLight 650. To assess cell binding and uptake, we incubated increasing concentrations of thermally equilibrated aptamers (Waz, E07, or C36) with cells in full culture media at 37°C, after which the cells were washed, trypsinized, and analyzed by flow cytometry. A plot of the ratio of median fluorescence of the signal to median fluorescence of the nontargeting aptamer, C36, demonstrated a clear dose response for both Waz and E07 (Figure 2A). A representative histogram for each set of assays performed at 1,000 nM on each cell line is also shown (Figure 2B). As expected, the non-targeting control, C36, showed little cell staining or uptake. Aptamer staining with Waz and E07 correlates with expression levels as assessed by antibody staining (Figure 1). That is, Panc-1 and MIA PaCa-2 cells demonstrated higher maximal binding of Waz than of E07, while BxPC3 cells demonstrated higher levels of staining with E07. The dose-response curves were used to determine the apparent dissociation constant ( $K_D$ ) and maximal binding ( $B_{max}$ ) for each aptamer on each cell line (Table 1).

### Synthesis and Characterization of Aptamer-Auristatin Conjugates

We generated aptamer-auristatin conjugates from the same thiol-modified aptamers used to generate the preceding dye-labeled conjugates. Conjugates were made using one of two thiol-reactive toxin variants: the membrane-permeable auristatin derivative MMAE bearing a cathepsin-cleavable valine-citrulline linker (MC-VC-PAB-MMAE) or the membrane-impermeable auristatin derivative MMAF (MC-MMAF) (Figure 3A). Reduced aptamers were incubated with a 3-fold molar excess of either MC-VC-PAB-MMAE or MC-MMAF. The progress of the reaction was monitored by reverse-phase high-performance liquid chromatography (HPLC) and routinely proceeded to 100% (Figure 3B). Conjugates were subsequently desalted, and their identities were confirmed by mass spectrometry (Figure 3C).

Because of the potential for the presence of the drug to interfere with aptamer binding function, we performed a competition binding experiment to ensure that drug conjugation did not adversely affect

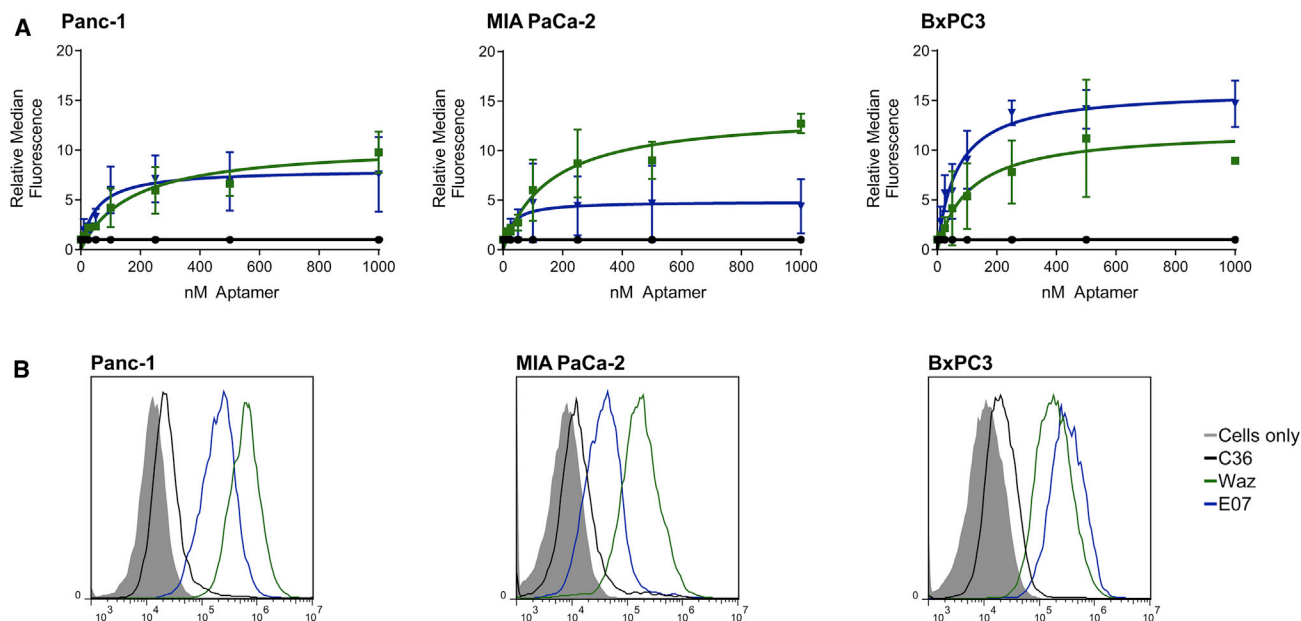


**Figure 2. Aptamer Binding and Uptake Characteristics of PDAC Cells**

(A) Flow cytometry data were used to produce a plot of relative median fluorescence versus aptamer concentration. Cells were incubated with increasing concentrations of DyLight 650-labeled Waz, E07, and nontargeting control C36. Aptamer binding was normalized to C36 to account for nonspecific uptake and was based on a minimum of three independent experiments. Apparent  $K_D$  values can be found in Table 2. (B) Cell binding and internalization of aptamers at 1,000 nM from one experiment are shown for reference.

aptamer function. DyLight 650-labeled aptamers (Waz or E07) were incubated with increasing concentrations of MMAE-, MMAF-, or Alexa Fluor 488 (AF488)-labeled aptamer. As shown in Figure 3D, both the drug conjugates and the dye conjugate demonstrate a similar ability to compete with DyLight 650 for binding, indicating that aptamer function is not adversely affected by drug conjugation.

Critical to the function of the targeted toxin is its ability to separate from the targeting ligand upon uptake and entry into the cytoplasm. The valine-citrulline dipeptide in MC-VC-PAB-MMAE renders it susceptible to degradation by cathepsin B in the acidic environment of the endosome. MC-MMAF, however, contains no such linkage. To validate this chemistry while conjugated to an aptamer, we incubated MMAE- and MMAF-conjugated aptamers both with cathepsin B in acidic buffer and without cathepsin B in neutral buffer. As shown in Figures 4A and S1, free aptamer can be readily distinguished from

both the MMAE and the MMAF conjugates on a 20% denaturing (7 M urea) polyacrylamide gel. Only aptamer-MMAE conjugates, not MMAF conjugates, incubated with cathepsin B under acidic conditions demonstrated an increase in electrophoretic mobility, indicating cleavage. No cleavage of MMAE was observed without cathepsin B at neutral pH.

Finally, although cathepsin B is known to be ubiquitous, with varied expression levels and distribution throughout the endosomes and lysosomes of most cells,<sup>24</sup> we performed a co-localization study using AF488-Waz and Magic Red, an activity-based probe that detects the presence of cathepsin B in cells. Following cellular uptake, the aptamer (Figure 4B, green) demonstrated characteristic punctate staining, consistent with localization to endosomal and lysosomal compartments that co-localized well with that of cathepsin B staining (Figure 4B, red).

**Table 1. Aptamer Sequences**

	Aptamer Sequences (5'-3')
C36	5S-GGCGUAGUGAUUAUGAAUCGUGUCUAAUACACGCC-t
Waz	5S-GGGUUCUACGAUAAACGGUUAUAGUACAGCUUAUGGCUGGC AGUUCCT-t
E07	5S-GGACGGAUUUAAUCGCCGUAGAAAGCAUGUCAAGCCGGAA CCGUCC-t

Sequences of Waz, E07, and the nontargeting control C36. 5S indicates a 5' thiol; t indicates an inverted dT or FAM. Aptamers were synthesized with 2'-fluoropyrimidines and 2'-hydroxyl purines.

#### Evaluation of Aptamer-Auristatin Conjugate Toxicity

We assessed the efficacy of our aptamer-targeted toxins on three PDAC cell lines. Cells were incubated with conjugates for 4 days, at which time toxin-containing media were replenished with fresh media. After an additional 2 days, toxicity was determined. All assays were performed using both free toxin and a nontargeting control-toxin conjugate (C36-MMAE/F).

Conjugates of Waz and E07 bearing the cathepsin-cleavable, membrane-permeable MC-VC-PAB-MMAE both resulted in improvement in cytotoxicity on the PDAC cell lines when compared to

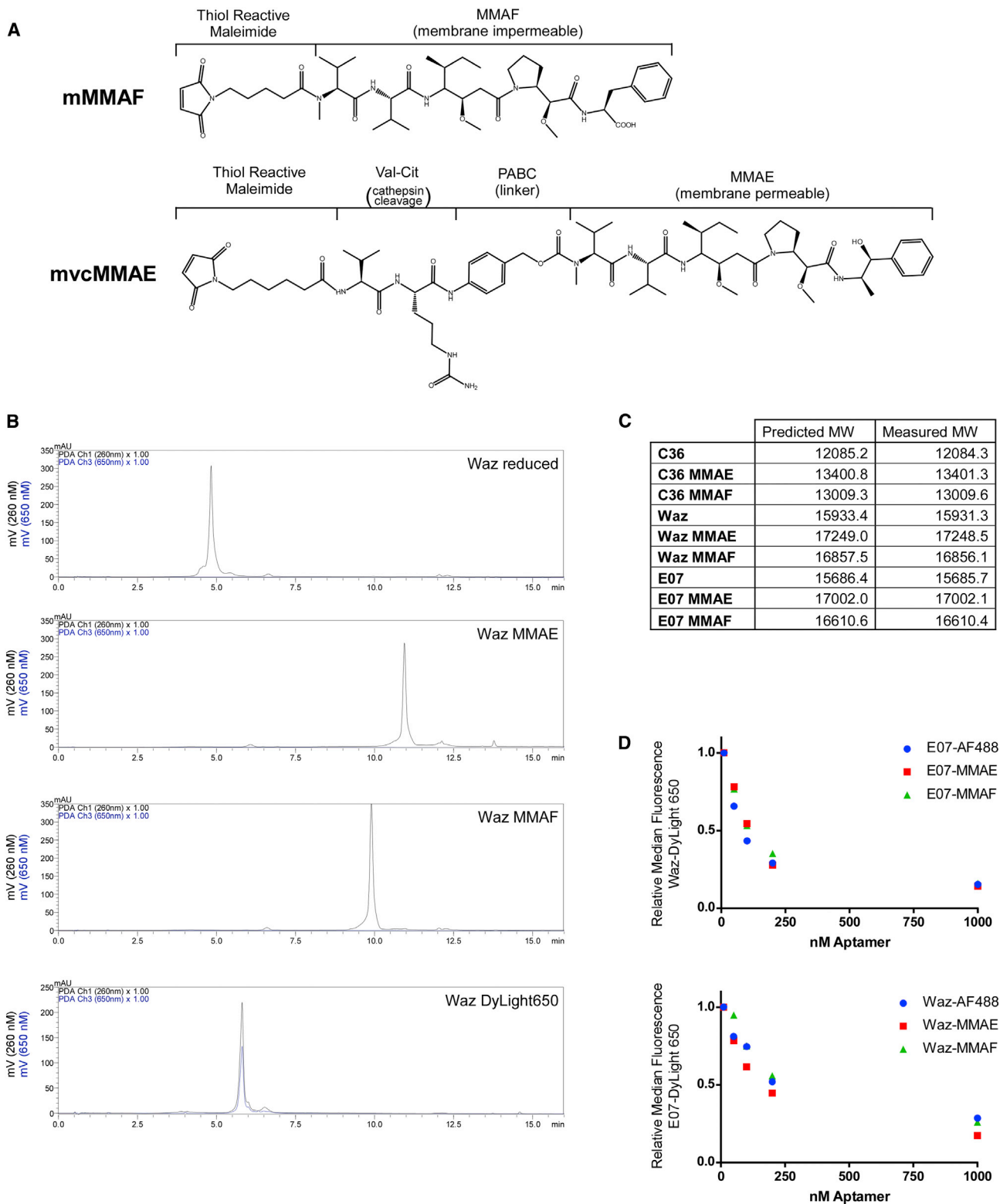


**Figure 3. Synthesis, Purification, and Characterization of Aptamer Auristatin Conjugates**

(A) Chemical structure of MMAE and MMAF used in our studies. MMAE includes the cleavable linker, valine-citrulline, and the self-immolative spacer, p-amino-benzyloxy carbonyl (PABC). (B) HPLC traces of Waz during reduction and conjugation. (Top panel) Analytical analysis of purified, reduced Waz. (2<sup>nd</sup> panel) Analysis of

(legend continued on next page)

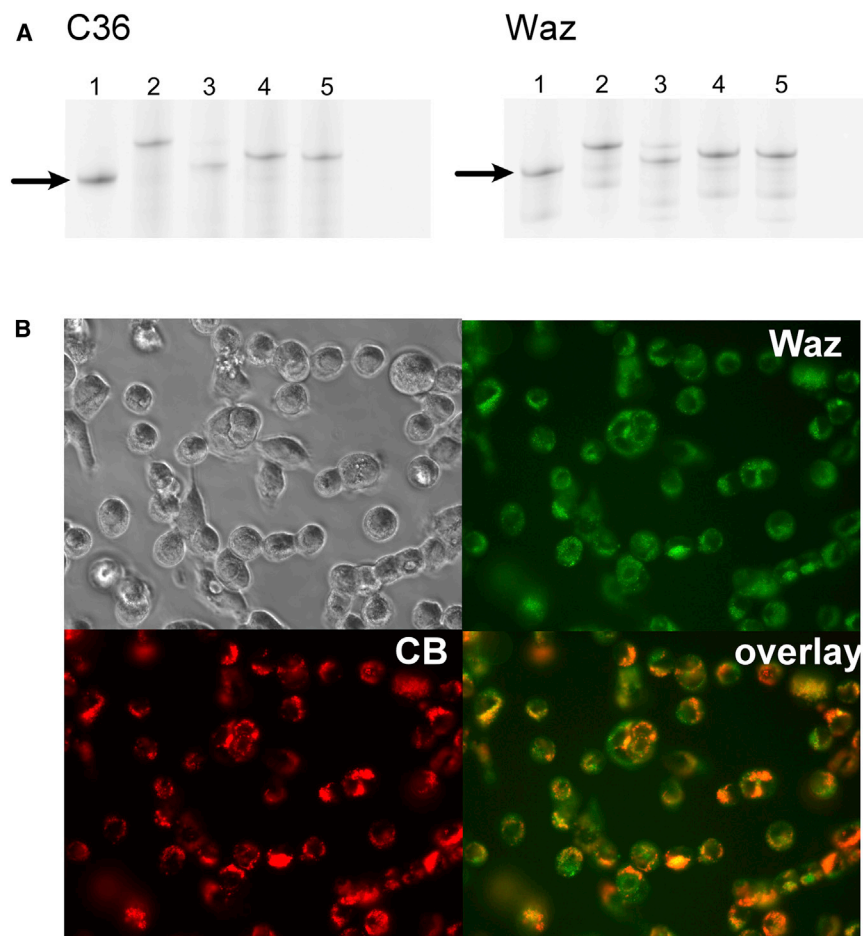


**Figure 4. Further Characterization of Aptamers and Aptamer Conjugates**

(A) Cleavage of aptamer-toxin conjugates in the presence of cathepsin B. Lane 1: aptamer reduced with 10 mM TCEP at 70°C for 10 m. Lane 2: aptamer-MMAE conjugate incubated in PBS<sup>-</sup> (pH 7). Lane 3: aptamer-MMAE conjugate incubated in PBS<sup>-</sup> (pH 4), with 0.1 mg/mL of cathepsin B. Lane 4: aptamer-MMAF conjugate incubated in PBS<sup>-</sup> (pH 7). Lane 5: aptamer-MMAF conjugate incubated in PBS<sup>-</sup> (pH 4), with 0.1 mg/mL of cathepsin B. Samples in lanes 2–5 were incubated for 24 hr at 37°C. Arrows indicate reduced, unconjugated aptamer. (B) Colocalization of Waz-AF488 (Waz; green) and cathepsin B (CB; red).

(51 nM), while the IC<sub>50</sub>s on Panc-1 and BxPC3 cells were somewhat higher (190 and 450 nM, respectively). Targeting EGFR provided the greatest toxicity on MIA PaCa-2 cells (220 nM) and had relatively less effect on BxPC3 cells (~1,000 nM) and Panc-1 cells (>1,000 nM). Consistent with its inability to cross the extracellular membrane, MMAF alone was significantly less toxic (~10-fold) than MMAE. Conjugation of MMAF to our nontargeting control aptamer rendered it even less toxic (>1,000 nM on Panc-1 and BxPC3 cells and ~950 nM on MIA PaCa-2 cells).

To ensure the mechanism of action of both Waz and E07 conjugates, we performed toxicity assays on B16 cells, a murine cell line for which

neither Waz nor E07 demonstrate any significant binding (Figure S2). Consistent with these data, no significant toxicity (IC<sub>50</sub> >1,000 nM) was observed using these constructs on these cells, a level similar to that seen using our non-targeted control, C36 (Table 3; Figure S3).

Finally, to ensure that the observed differences in cell death were not a result of conjugate degradation and drug release over the course of the assay, we performed a stability assay using fluorescently labeled aptamers in culture media. Little difference in stability was observed (Figure S4).

## DISCUSSION

Aptamer-toxin conjugates have the potential to improve the therapeutic index of chemotherapeutics by targeting toxins to cancer cells while bypassing healthy cells. Their small size abets tissue penetration, and their rapid clearance may improve off-target effects, a

toxicity of a nontargeting control, C36-MMAE (Figure 5). Conjugates targeting TfR (Waz-MMAE) demonstrated the greatest increase in cytotoxicity when compared to the negative control. On all three cell lines, Waz-MMAE conjugates displayed half-maximal inhibitory concentration (IC<sub>50</sub>) values of ~35 nM, while conjugates targeting EGFR proved somewhat less toxic and demonstrated a more varied response: IC<sub>50</sub> of 55 nM on PANC-1 cells and ~120 nM on MIA PaCa-2 and BxPC3 cells (Table 3). Consistent with its ability to enter cells on its own, free MMAE yielded the lowest observed IC<sub>50</sub> values across all three cell lines.

Similar experiments were performed with conjugates generated using the non-membrane-permeable MMAF-toxin conjugates. As shown in Figure 5 and summarized in Table 3, results with MMAF were somewhat more varied across cell types. Targeting TfR proved the most toxic: the IC<sub>50</sub> on MIA PaCa-2 cells was relatively low

MMAE-conjugated Waz. (3<sup>rd</sup> panel) Analysis of MMAF-conjugated Waz. (Bottom panel) Analysis of DyLight 650-conjugated Waz. A shift in the observable product, absence of a second peak, and superimposition of the 260 and 650 traces for DyLight 650 indicate >99% conjugation. Reduction, conjugation, and removal of excess dye or toxin were performed as described in Materials and Methods. (C) Comparison of predicted and measured molecular weights of aptamers and aptamer-toxin conjugates. Mass spectrometry was used to measure the molecular weight of aptamers and aptamer-toxin conjugates. (D) Competition analysis of dye and toxin (MMAE or MMAF)-labeled aptamers. Constructs tested are as indicated. Assay was performed as described in Materials and Methods.

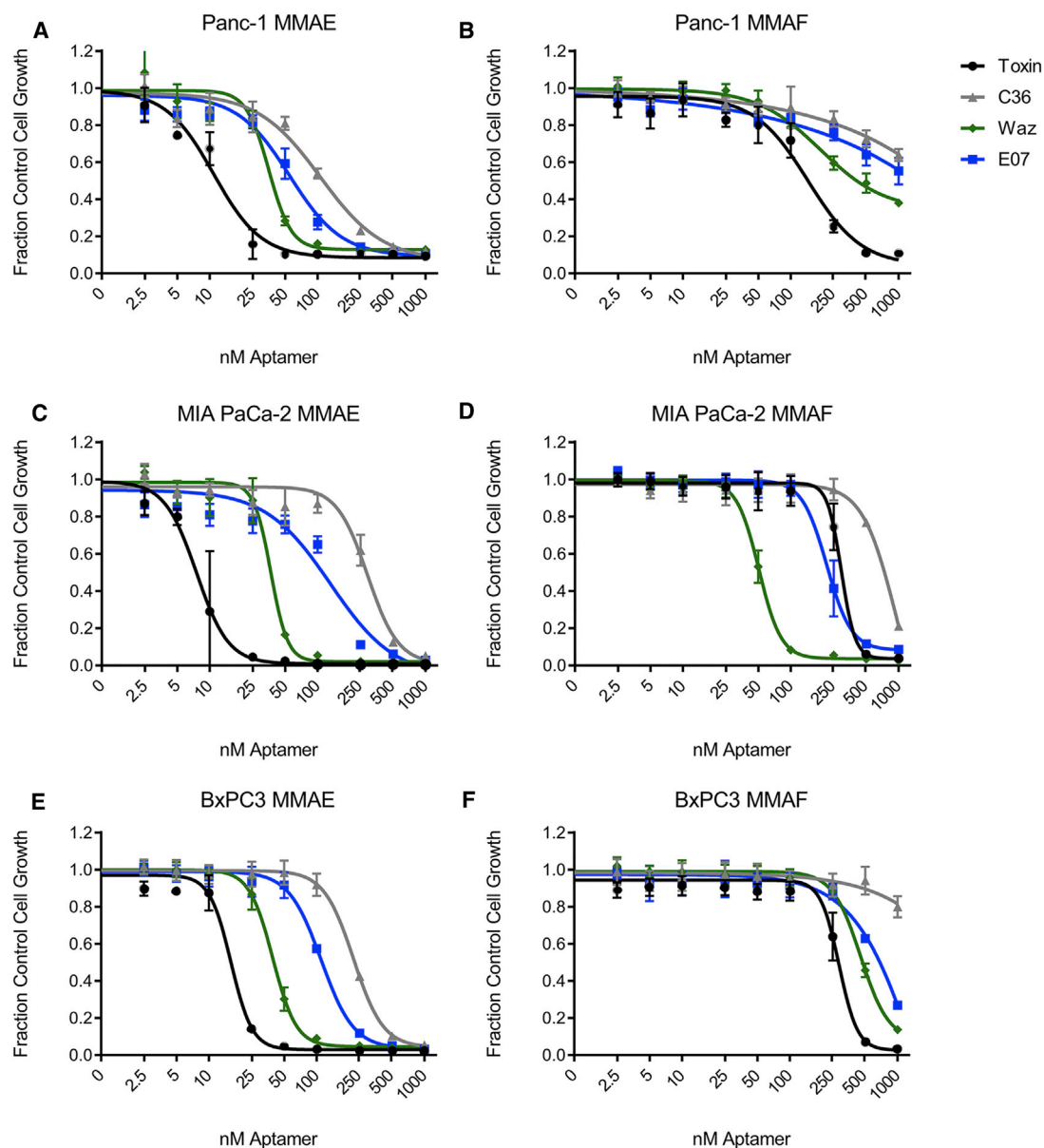


**Figure 5. Cytotoxicity of Aptamer-Toxin Conjugates**

(A–F) Panc-1 (A and B), MIA PaCa-2 (C and D), and BxPC3 (E and F) cells were incubated with increasing concentrations of C36, Waz, and E07 conjugated to MMAE (A, C, and E) or MMAF (B, D, and F), as well as toxin alone. Assays were performed in growth media containing 10% FBS and preblocked with 1.0 mg/mL of ssDNA for 1 hr. Conjugates were incubated on cells for 4 days, and then cells were allowed to recover in fresh media for an additional 2 days before assaying. IC<sub>50</sub> values for each aptamer-toxin conjugate and cell combination can be found in Table 3.

potential consequence of the long half-lives of antibodies.<sup>25,26</sup> Perhaps more importantly, as chemicals, aptamers may simplify drug development, removing the biological component (i.e., the antibody) and providing a facile means for site-specific conjugation.

Previously, we streamlined conjugation of an aptamer to a protein toxin by chemically synthesizing a minimized aptamer bearing a 5' thiol and generating an activated pyridyl disulfide for subsequent

toxin conjugation.<sup>21</sup> Here, we exploited the maleimide functional groups on commercially available MMAE and MMAF derivatives to further simplify the process of conjugating aptamers to these small molecule toxins. Unlike our previous work, these aptamer-small molecule toxin conjugates are chemicals, not biologics.

Based on the observation that many PDACs overexpress TfR and EGFR, we assessed the ability to use anti-TfR and anti-EGFR

**Table 2. Apparent  $K_D$  and  $B_{max}$  of Aptamers on PDAC Cell Lines**

	Apparent $K_D$ (nM)		$B_{max}$ (Relative Units)	
	Waz	E07	Waz	E07
Panc-1	170 ± 59	51 ± 22	10 ± 1.2	8.1 ± 0.87
MIA PaCa-2	160 ± 42	26 ± 20	14 ± 1.3	4.9 ± 0.79
BxPC3	110 ± 66	67 ± 16	12 ± 2.4	16 ± 1.0
B16	>1,000	>1,000	0.89 ± 0.10	0.83 ± 0.10

Aptamer dose-response curves were used to determine the apparent  $K_D$  for Waz and E07 on Panc-1, MIA PaCa-2, BxPC3, and B16 cells. Apparent  $K_D$  values are shown in nanomolars,  $B_{max}$  values are shown in relative units, and both were calculated based on a plot of the median fluorescence normalized to the fluorescence of C36 to account for nonspecific uptake. Results are based on a minimum of three independent experiments.

aptamers to target auristatin derivatives to three PDAC cell lines: Panc-1, MIA PaCa-2, and BxPC3. In initial experiments, we validated receptor expression by flow cytometry using commercial antibodies and two aptamers: the anti-human TfR (hTfR) aptamer, Waz,<sup>19</sup> and a minimized variant of the anti-EGFR aptamer, E07.<sup>18</sup> Antibody binding data showed that Panc-1 and MIA PaCa-2 cells expressed slightly more TfR while BxPC3 cells expressed slightly more EGFR, a trend that is paralleled in the maximal binding observed for the aptamers on these cell lines (compare Figures 1 and 2). The aptamers demonstrate specific, saturable binding when compared to assays performed using a non-specific control aptamer sequence, C36. The apparent  $K_D$  of E07 on all three PDAC cell lines was less than 100 nM. The apparent  $K_D$  of Waz was generally higher and showed some variation (Figure 2; Table 2). The B16 mouse melanoma cell line, chosen as a negative control, did not express human TfR or EGFR and did not bind Waz or E07 aptamers (Figure S2).

We generated aptamer-toxin conjugates using two derivatives of auristatin: MMAE, a membrane-permeable variant, and MMAF, a less potent, membrane-impermeable variant. Both were conjugated to aptamers using thiol-maleimide coupling. In the case of MMAE, the construct also contained a cathepsin-cleavable linker (MC-VC-PAB-MMAE), which provides an endosomal release mechanism. While this mechanism of cleavage is well documented for antibody-based drugs, we were unsure whether the presence of the aptamer, a polyanion, would interfere with this process and thus confirmed cleavage using recombinant cathepsin B under acidic conditions (Figure 3), suggesting cleavage can also occur *in vitro* following endocytosis.

Although Waz demonstrated weaker affinity for binding to the PDAC cell lines than E07 (apparent  $K_D$  = ~110–170 nM versus 20–50 nM) (Table 2), all Waz conjugates displayed lower  $IC_{50}$  values than those of the E07 conjugates. This result is likely a consequence of multiple factors, including the number of cell surface receptors, rates of receptor internalization and turnover, and the route of trafficking, which may differ in different lines and for different pathways, rendering them more or less toxic. Because migration of the toxin to the cytoplasm is critical for function, limits on the rate of release from

the aptamer or the endosome will affect the observed toxicity. For example, in the case of the protein toxin, gelonin, endosomal escape is the rate-limiting step in ligand-targeted delivery, not ligand binding or conjugate internalization.<sup>27</sup>

In the case of the MC-VC-PAB-MMAE conjugates, in which the MMAE toxin is membrane permeable following cleavage, the rate-limiting step may be processing within the endosome. In the case of membrane-impermeable MMAF, following uptake, toxicity is likely a consequence of both aptamer degradation and endosomal escape, processes that are likely different for different cell lines and different uptake pathways.

Although the  $IC_{50}$ s of aptamer-MMAE conjugates were consistently lower than those of aptamer-MMAF conjugates, killing by the non-targeting control C36-MMAE was significant, resulting in a relatively low therapeutic index for these conjugates on PDAC cells even though killing of off-target B16 cells was negligible (Figure 5; Figure S3; Table 3). Aptamer-MMAF conjugates, however, while less toxic, demonstrated a much larger therapeutic index on PDAC cells and again, negligible killing on B16 cells. MMAE is a more toxic molecule than MMAF,<sup>28</sup> which may partially explain this result. In addition, once released, MMAE can permeate the cellular membrane to kill other cells (i.e., the bystander effect). *In vivo*, the bystander effect can help kill surrounding cells in the tumor.<sup>29,30</sup> However, *in vitro*, it may have inadvertently lowered the  $IC_{50}$  of C36-MMAE.

We acknowledge that this work only examines two variants of the auristatins. When we initiated this work, MMAE was only commercially available conjugated to the cathepsin B-cleavable valine-citrulline dipeptide linker and MMAF was only supplied conjugated to a non-cleavable linker. This had the effect of coupling cell permeability (MMAE is cell permeable; MMAF is not) with linker cleavability. MMAE and MMAF are now commercially available with a variety of linkers: non-cleavable MMAE and cleavable MMAF, as well as substitutions for the valine-citrulline linkage to other dipeptide linkages<sup>28</sup> and substitutions for the maleimidocaproyl to a bromoacetamidocaproyl.<sup>25</sup> These substitutions have been shown to directly affect the therapeutic index of antibody-auristatin conjugates.<sup>25,28</sup> Moving forward, we aim to explore the effect of these new linker chemistries on the toxicity of aptamer-drug conjugates. We hypothesize that MMAF conjugated to a cathepsin B-cleavable linker holds particular promise. Though MMAF is less toxic than MMAE, its inability to cross the lipid bilayer into other cells, coupled with its higher aqueous solubility,<sup>31</sup> should result in an improved therapeutic index *in vitro* if endosomal escape can be facilitated by a cleavable linker. However, the behavior of different toxin variants on different cell lines appears idiosyncratic and likely must be determined empirically.<sup>25,31,32</sup>

Finally, it is worth comparing our work to a publication by Yoon et al.<sup>33</sup> In that work, the authors took advantage of another important aspect of aptamers: the ability to use them agnostically to target-specific cell types without prior knowledge of specific surface receptors. The authors adapted a previously reported anti-PDAC aptamer,

**Table 3. IC<sub>50</sub> of Aptamer-Toxin Conjugates on PDAC Cell Lines**

		Toxin (nM)	C36 (nM)	Waz (nM)	E07 (nM)
Panc-1	MMAE	11 (8.9–13)	110 (76–148)	35 (31–41)	55 (44–69)
	MMAF	140 (110–190)	>1,000	190 (130–280)	>1,000
MIA PaCa-2	MMAE	7.5 (6.5–8.7)	290 (250–340)	37 (33–41)	130 (90–190)
	MMAF	290 (260–340)	940 (190–>1,000)	51 (49–53)	220 (200–240)
BxPC3	MMAE	16 (15–18)	220 (200–240)	39 (37–41)	110 (100–120)
	MMAF	290 (0–320)	>1,000	450 (410–530)	>1,000 (480–>1,000)
B16	MMAE	56 (46–69)	>1,000	>1,000	>1,000
	MMAF	>1,000	>1,000	>1,000	>1,000

The IC<sub>50</sub> values of aptamer-toxin conjugates, nontargeting control-toxin conjugates, and toxin alone on PDAC cells lines are reported in nanomolars, including the 95% confidence interval. Results are based on three discrete measurements at each concentration.

P19, and demonstrated its ability to target and deliver the auristatin MMAE and a derivative of maytansine (DM1). The toxins were attached to a short oligonucleotide and then to the aptamer via hybridization, unlike the direct conjugation strategy we employed here. In that study, dose-dependent killing with the targeted toxin was also observed. Altogether, these results bode well for the development and further optimization of aptamer-small molecule toxin conjugations for the treatment of PDAC, as well as other cancers.

In summary, aptamer-auristatin conjugates are quickly and reliably synthesized and prove toxic to PDAC cells. Here, we assayed the anti-transferrin aptamer, Waz, and the anti-EGFR aptamer, E07, conjugated to MMAE and MMAF on three PDAC cell lines. Our results show that the best aptamer for targeted delivery of a toxin to a cell line cannot be chosen based on binding alone. While aptamer-MMAE conjugates displayed low IC<sub>50</sub> values across all three cell lines, C36-MMAE conjugates were correspondingly low, suggesting a rather narrow therapeutic window. The largest therapeutic window was found for MMAF conjugates. Future work should attempt to improve aptamer stability for *in vivo* use and explore different linker and toxin combinations. While the literature has given considerable attention to ADCs for the treatment of PDAC, our data suggest that aptamer-drug conjugates are a viable alternative with many potential advantages.

## MATERIALS AND METHODS

### Cells and Media

Cells were purchased from ATCC and maintained at 37°C with 5% CO<sub>2</sub> and 99% humidity. Panc-1, MIA PaCa-2, and B16 cells were maintained in DMEM supplemented with 10% fetal bovine serum (FBS). BxPC3 cells were maintained in RPMI supplemented with 10% FBS.

### Aptamer Synthesis and Labeling

Aptamers were synthesized in house via solid-phase synthesis on an Expedite 8909 DNA synthesizer (BioLytic Lab Performance, Fremont, CA). Phosphoramidite monomers (2'-hydroxyl A/G, 2'-fluoro-modified C/U) were purchased from ChemGenes (Wilmington, MA). All other synthesis reagents were purchased from Glen Research

(Sterling, VA). Aptamers were synthesized on an inverted dT or fluorescein (FAM) controlled pore glass (CPG) column (where indicated) bearing a 5' thiol modification using a thiol modifier, C6 S-S phosphoramidite. The final 5' dimethoxytrityl group was left on to facilitate purification. Aptamer sequences can be found in Table 2. Following cleavage and deprotection, aptamers were purified by reversed-phase HPLC on a 10 × 50 mm Xbridge C18 column (Waters, Milford, MA) using a linear gradient of acetonitrile in 0.1 M triethylammonium acetate (TEAA) at 7.5.

Aptamers in 0.1 M TEAA were reduced with 10 mM Tris (2-chloroethyl) phosphate (TCEP) by heating to 70°C for 10 min and cooling for 1 hr at room temperature. Reduction was confirmed by HPLC. TCEP was removed by buffer exchanging into PBS<sup>-</sup> using a 10 K concentrator (Millipore, Ireland). Reduced aptamers were incubated for 1 hr at room temperature with a 3- to 5-fold molar excess of maleimide-labeled DyLight 650 (Thermo Fisher Scientific, Waltham, MA), AF488 (Life Technologies, Carlsbad, CA), MC-VC-PAB-MMAE (Concortis Biosystems, San Diego, CA), or MC-MMAF (Concortis Biosystems). Conjugation was confirmed via HPLC and routinely proceeded to 100%. Excess dye and toxin were removed by buffer exchanging into PBS<sup>-</sup> using a 10 K concentrator (Millipore).

The identity of the labeled aptamers was confirmed by liquid chromatography-mass spectrometry (LC-MS), using a Waters Acquity ultra-performance liquid chromatography (UPLC) system coupled to a Waters Synapt G2 quadrupole-time-of-flight hybrid mass spectrometer. For analysis, aptamers were resuspended at 200 μM in PBS<sup>-</sup>. Approximately 5 μL of each sample was desalted using a linear gradient of MeOH in 400 mM hexafluoroisopropanol (HFIP)/8 mM triethylamine (TEA) using a Waters Xbridge C18 2.1 × 50 mm column. The resulting mass spectra were deconvoluted using MagTran.<sup>34</sup>

### Antibody and Aptamer Binding Assays

To determine antibody binding, cells were washed in PBS<sup>-</sup> and lifted with 0.5% trypsin, and 50,000 per well were stained with PE-labeled anti-TfR antibody (Catalog No. 2270530, Sony Biotechnology, San

Jose, CA), anti-EGFR antibody (Catalog No. 2364520, Sony Biotechnology), or the appropriate isotype controls (Catalog Nos. 2601060 and 2600560, Sony Biotechnology). Staining was performed in 100  $\mu$ L of Hank's balanced salt solution (HBSS) with 1% BSA and 0.1% sodium azide (fluorescence-activated cell sorting [FACS] buffer) for 30 min. Cells were then washed twice with FACS buffer, pelleted in a swinging-bucket centrifuge at  $300 \times g$  for 5 min, and resuspended in FACS buffer with 100 ng/mL of bisbenzimidazole to distinguish live from dead cells. Cells were read on an iCyt Eclipse EC800 flow cytometer, and data were analyzed using FlowJo.

To determine aptamer binding, cells were seeded at 50,000 cells per well in a 96 well tissue culture plate. The following day, 90  $\mu$ L of fresh media containing 1.0 mg/mL of DNA, sodium salt, and salmon testes (single-stranded DNA [ssDNA]; Millipore, Billerica, MA) was added to the cells and allowed to incubate for 1 hr. DyLight 650-labeled aptamers were prepared as  $10\times$  stocks in PBS<sup>-</sup>, heated to 70°C for 3 min, and allowed to renature at room temperature for 15 min. Aptamers were then added to cells and incubated for 1 hr at 37°C. Media were removed, and cells were washed twice with 100  $\mu$ L of PBS<sup>-</sup> and lifted with 0.5% trypsin. FACS buffer was added to inactivate the trypsin, and cells were pelleted by centrifugation and resuspended in FACS buffer with bisbenzimidazole. Cells were read on an iCyt Eclipse EC800 flow cytometer, and data were analyzed using FlowJo.

#### Aptamer Competition Assays

MIA PaCa-2 cells were washed in PBS<sup>-</sup> and lifted in 0.5% trypsin, and 50,000 per well were suspended in FACS buffer with 1.0 mg/mL of ssDNA for 30 min. DyLight 650-, AF488-, MMAE-, and MMAF-conjugated aptamers were prepared as  $20\times$  stocks, heated to 70°C for 3 min, and allowed to renature at room temperature for 15 min. To confirm that conjugating to DyLight 650, MMAE, or MMAF did not perturb aptamer binding, DyLight 650-labeled aptamer was mixed with the same aptamer labeled with AF488, MMAE, or MMAF and then added to cells. The final concentration on cells of DyLight 650-labeled aptamer was held constant at 100 nM, while the concentration of AF488-, MMAE-, and MMAF-labeled aptamer ranged from 10 to 1,000 nM. Aptamers were incubated with cells for 30 min, after which they were pelleted in a swinging-bucket centrifuge at  $300 \times g$  for 5 min, washed twice in FACS buffer, and resuspended in FACS buffer with 100 ng/mL of bisbenzimidazole to distinguish live from dead cells.

#### Cathepsin B Assay

Assay for cathepsin B cleavage was modified from Koga et al.<sup>11</sup> 50 ng of FAM-labeled aptamer-toxin conjugates were incubated for 24 hr at 37°C in either PBS<sup>-</sup> (pH 7) or PBS<sup>-</sup> (pH 4) with 0.1 mg/mL of cathepsin B (Athens Research & Technology, Athens, GA). Conjugates were run on a 20% polyacrylamide denaturing gel and imaged using a Storm 840 imaging system (GE Healthcare, Marlborough, MA).

#### Microscopy

Cells were seeded at 50,000 cells per well in an 8 well Lab-Tek chambered cover glass (Thermo Fisher Scientific). The following day,

180  $\mu$ L of fresh media containing 1.0 mg/mL of DNA, sodium salt, and salmon testes (ssDNA; Millipore, Billerica, MA) was added to the cells and allowed to incubate for 1 hr. Aptamers were added to cells at a final concentration of 500  $\mu$ M, and Magic Red cathepsin B assay (ImmunoChemistry Technologies, Bloomington, MN) was added to cells at the manufacturer's recommended concentration. After 1 hr, cells were washed twice with PBS<sup>-</sup> and imaged at  $60\times$  using a Nikon Eclipse Ti 90.

#### Evaluation of Aptamer-Auristatin Conjugate Toxicity

Cells were seeded at 4,000 cells per well in a 96 well tissue culture plate. The following day, cells were blocked for 1 hr with 90  $\mu$ L of fresh media containing 1.0 mg/mL of ssDNA and 1% penicillin-streptomycin. Aptamer-toxin conjugates were prepared as  $10\times$  stocks in Dulbecco PBS (DPBS), heated to 70°C for 3 min, and renatured at room temperature for 15 min. MMAE and MMAF (MedChem Express, Princeton, NJ) were prepared as  $5,000\times$  stocks in DMSO and then diluted to  $10\times$  in DPBS. Aptamer-toxin conjugates and toxins alone were added, and cells were incubated at 37°C with 5% CO<sub>2</sub> and 99% humidity. After 4 days, toxin-containing media were replaced by fresh media. After 2 additional days, cell viability was assayed with AlamarBlue (Invitrogen, Carlsbad, CA). Half-maximal inhibitory concentration (IC<sub>50</sub>) was determined using the variable slope model in GraphPad Prism 7 software.

#### SUPPLEMENTAL INFORMATION

Supplemental Information includes Supplemental Materials and Methods and four figures and can be found with this article online at <https://doi.org/10.1016/j.omtn.2017.11.013>.

#### AUTHOR CONTRIBUTIONS

C.K. conducted all experiments. Methods and approaches were conceived by C.K. and M.L.

#### ACKNOWLEDGMENTS

We thank Brian Weinrick for mass spectrometry. This work was supported by an MSTP training grant (T32-GM007288), the National Cancer Institute of the National Institutes of Health under award number R21 CA182330, and a Stand Up To Cancer (SU2C) Innovative Research Grant (IRG).

#### REFERENCES

1. Siegel, R.L., Miller, K.D., and Jemal, A. (2016). Cancer statistics, 2016. *CA Cancer J. Clin.* 66, 7–30.
2. Heinemann, V., and Boeck, S. (2008). Perioperative management of pancreatic cancer. *Ann. Oncol.* 19 (Suppl 7), vii273–vii278.
3. Burris, H.A., 3rd, Moore, M.J., Andersen, J., Green, M.R., Rothenberg, M.L., Modiano, M.R., Cripps, M.C., Portenoy, R.K., Stormiolo, A.M., Tarassoff, P., et al. (1997). Improvements in survival and clinical benefit with gemcitabine as first-line therapy for patients with advanced pancreas cancer: a randomized trial. *J. Clin. Oncol.* 15, 2403–2413.
4. Arslan, C., and Yalcin, S. (2014). Current and future systemic treatment options in metastatic pancreatic cancer. *J. Gastrointest. Oncol.* 5, 280–295.

5. Bai, R., Pettit, G.R., and Hamel, E. (1990). Dolastatin 10, a powerful cytostatic peptide derived from a marine animal. Inhibition of tubulin polymerization mediated through the vinca alkaloid binding domain. *Biochem. Pharmacol.* *39*, 1941–1949.
6. Sievers, E.L., and Senter, P.D. (2013). Antibody-drug conjugates in cancer therapy. *Annu. Rev. Med.* *64*, 15–29.
7. Remillard, S., Rebhun, L.L., Howie, G.A., and Kupchan, S.M. (1975). Antimitotic activity of the potent tumor inhibitor maytansine. *Science* *189*, 1002–1005.
8. Donaghy, H. (2016). Effects of antibody, drug and linker on the preclinical and clinical toxicities of antibody-drug conjugates. *MAbs* *8*, 659–671.
9. Amiri-Kordestani, L., Blumenthal, G.M., Xu, Q.C., Zhang, L., Tang, S.W., Ha, L., Weinberg, W.C., Chi, B., Candau-Chacon, R., Hughes, P., et al. (2014). FDA approval: ado-trastuzumab emtansine for the treatment of patients with HER2-positive metastatic breast cancer. *Clin. Cancer Res.* *20*, 4436–4441.
10. Casi, G., and Neri, D. (2012). Antibody-drug conjugates: basic concepts, examples and future perspectives. *J. Control. Release* *161*, 422–428.
11. Koga, Y., Manabe, S., Aihara, Y., Sato, R., Tsumura, R., Iwafuji, H., Furuya, F., Fuchigami, H., Fujiwara, Y., Hisada, Y., et al. (2015). Antitumor effect of antitissue factor antibody-MMAE conjugate in human pancreatic tumor xenografts. *Int. J. Cancer* *137*, 1457–1466.
12. Scales, S.J., Gupta, N., Pacheco, G., Firestein, R., French, D.M., Koeppen, H., Rangell, L., Barry-Hamilton, V., Luis, E., Chuh, J., et al. (2014). An antimesothelin-monomethyl auristatin e conjugate with potent antitumor activity in ovarian, pancreatic, and mesothelioma models. *Mol. Cancer Ther.* *13*, 2630–2640.
13. Buckel, L., Savariar, E.N., Crisp, J.L., Jones, K.A., Hicks, A.M., Scanderbeg, D.J., Nguyen, Q.T., Sicklick, J.K., Lowy, A.M., Tsien, R.Y., and Advani, S.J. (2015). Tumor radiosensitization by monomethyl auristatin E: mechanism of action and targeted delivery. *Cancer Res.* *75*, 1376–1387.
14. Troiani, T., Martinelli, E., Capasso, A., Morgillo, F., Orditura, M., De Vita, F., and Ciardiello, F. (2012). Targeting EGFR in pancreatic cancer treatment. *Curr. Drug Targets* *13*, 802–810.
15. Ryschich, E., Huszty, G., Knaebel, H.P., Hartel, M., Büchler, M.W., and Schmidt, J. (2004). Transferrin receptor is a marker of malignant phenotype in human pancreatic cancer and in neuroendocrine carcinoma of the pancreas. *Eur. J. Cancer* *40*, 1418–1422.
16. Ueda, S., Ogata, S., Tsuda, H., Kawarabayashi, N., Kimura, M., Sugiura, Y., Tamai, S., Matsubara, O., Hatsuse, K., and Mochizuki, H. (2004). The correlation between cytoplasmic overexpression of epidermal growth factor receptor and tumor aggressiveness: poor prognosis in patients with pancreatic ductal adenocarcinoma. *Pancreas* *29*, e1–e8.
17. Jeong, S.M., Hwang, S., and Seong, R.H. (2016). Transferrin receptor regulates pancreatic cancer growth by modulating mitochondrial respiration and ROS generation. *Biochem. Biophys. Res. Commun.* *471*, 373–379.
18. Li, N., Nguyen, H.H., Byrom, M., and Ellington, A.D. (2011). Inhibition of cell proliferation by an anti-EGFR aptamer. *PLoS ONE* *6*, e20299.
19. Maier, K.E., Jangra, R.K., Shieh, K.R., Cureton, D.K., Xiao, H., Snapp, E.L., Whelan, S.P., Chandran, K., and Levy, M. (2016). A new transferrin receptor aptamer inhibits new world hemorrhagic fever mammarenavirus entry. *Mol. Ther. Nucleic Acids* *5*, e321.
20. Ray, P., Cheek, M.A., Sharaf, M.L., Li, N., Ellington, A.D., Sullenger, B.A., Shaw, B.R., and White, R.R. (2012). Aptamer-mediated delivery of chemotherapy to pancreatic cancer cells. *Nucleic Acid Ther.* *22*, 295–305.
21. Kelly, L., Kratschmer, C., Maier, K.E., Yan, A.C., and Levy, M. (2016). Improved synthesis and in vitro evaluation of an aptamer ribosomal toxin conjugate. *Nucleic Acid Ther.* *26*, 156–165.
22. Ali, S., El-Rayes, B.F., Sarkar, F.H., and Philip, P.A. (2005). Simultaneous targeting of the epidermal growth factor receptor and cyclooxygenase-2 pathways for pancreatic cancer therapy. *Mol. Cancer Ther.* *4*, 1943–1951.
23. Sugyo, A., Tsuji, A.B., Sudo, H., Okada, M., Koizumi, M., Satoh, H., Kurosawa, G., Kurosawa, Y., and Saga, T. (2015). Evaluation of efficacy of radioimmunotherapy with 90Y-labeled fully human anti-transferrin receptor monoclonal antibody in pancreatic cancer mouse models. *PLoS One* *10*, e0123761.
24. Mohamed, M.M., and Sloane, B.F. (2006). Cysteine cathepsins: multifunctional enzymes in cancer. *Nat. Rev. Cancer* *6*, 764–775.
25. Alley, S.C., Benjamin, D.R., Jeffrey, S.C., Okeley, N.M., Meyer, D.L., Sanderson, R.J., and Senter, P.D. (2008). Contribution of linker stability to the activities of anticancer immunoconjugates. *Bioconjug. Chem.* *19*, 759–765.
26. de Claro, R.A., McGinn, K., Kwitkowski, V., Bullock, J., Khandelwal, A., Habtemariam, B., Ouyang, Y., Saber, H., Lee, K., Koti, K., et al. (2012). U.S. Food and Drug Administration approval summary: brentuximab vedotin for the treatment of relapsed Hodgkin lymphoma or relapsed systemic anaplastic large-cell lymphoma. *Clin. Cancer Res.* *18*, 5845–5849.
27. Pirie, C.M., Hackel, B.J., Rosenblum, M.G., and Wittrup, K.D. (2011). Convergent potency of internalized gelonin immunotoxins across varied cell lines, antigens, and targeting moieties. *J. Biol. Chem.* *286*, 4165–4172.
28. Doronina, S.O., Bovee, T.D., Meyer, D.W., Miyamoto, J.B., Anderson, M.E., Morris-Tilden, C.A., and Senter, P.D. (2008). Novel peptide linkers for highly potent antibody-auristatin conjugate. *Bioconjug. Chem.* *19*, 1960–1963.
29. Li, F., Emmerton, K.K., Jonas, M., Zhang, X., Miyamoto, J.B., Setter, J.R., Nicholas, N.D., Okeley, N.M., Lyon, R.P., Benjamin, D.R., and Law, C.L. (2016). Intracellular released payload influences potency and bystander-killing effects of antibody-drug conjugates in preclinical models. *Cancer Res.* *76*, 2710–2719.
30. Kovtun, Y.V., Audette, C.A., Ye, Y., Xie, H., Ruberti, M.F., Phinney, S.J., Leece, B.A., Chittenden, T., Blättler, W.A., and Goldmacher, V.S. (2006). Antibody-drug conjugates designed to eradicate tumors with homogeneous and heterogeneous expression of the target antigen. *Cancer Res.* *66*, 3214–3221.
31. Doronina, S.O., Mendelsohn, B.A., Bovee, T.D., Cerveny, C.G., Alley, S.C., Meyer, D.L., Oflazoglu, E., Toki, B.E., Sanderson, R.J., Zabinski, R.F., et al. (2006). Enhanced activity of monomethylauristatin F through monoclonal antibody delivery: effects of linker technology on efficacy and toxicity. *Bioconjug. Chem.* *17*, 114–124.
32. Srinivasarao, M., Galliford, C.V., and Low, P.S. (2015). Principles in the design of ligand-targeted cancer therapeutics and imaging agents. *Nat. Rev. Drug Discov.* *14*, 203–219.
33. Yoon, S., Huang, K.-W., Reebye, V., Spalding, D., Przytycka, T.M., Wang, Y., Swiderski, P., Li, L., Armstrong, B., Reccia, I., et al. (2017). Aptamer-drug conjugates of active metabolites of nucleoside analogs and cytotoxic agents inhibit pancreatic tumor cell growth. *Mol. Ther. Nucleic Acids* *6*, 80–88.
34. Zhang, Z., and Marshall, A.G. (1998). A universal algorithm for fast and automated charge state deconvolution of electrospray mass-to-charge ratio spectra. *J. Am. Soc. Mass Spectrom.* *9*, 225–233.